BioOne COMPLETE

A DNA Double-Strand Break Kinetic Rejoining Model Based on the Local Effect Model

Authors: Tommasino, F., Friedrich, T., Scholz, U., Taucher-Scholz, G., Durante, M., et al.

A DNA Double-Strand Break Kinetic Rejoining Model Based on the Local Effect Model

F. Tommasino,[a] T. Friedrich,[a] U. Scholz,[a] G. Taucher-Scholz,[a] M. Durante[a,b] and M. Scholz[a,1]

[a] GSI Helmholtzzentrum für Schwerionenforschung, Department of Biophysics, Darmstadt, Germany; and [b] Technische Universität Darmstadt, Institut für Festkörperphysik, Darmstadt, Germany

Tommasino, F., Friedrich, T., Scholz, U., Taucher-Scholz, G., Durante, M. and Scholz, M. A DNA Double-Strand Break Kinetic Rejoining Model Based on the Local Effect Model. *Radiat. Res*. 180, 524–538 (2013).

We report here on a DNA double-strand break (DSB) kinetic rejoining model applicable to a wide range of radiation qualities based on the DNA damage pattern predicted by the local effect model (LEM). In the LEM this pattern is derived from the SSB and DSB yields after photon irradiation in combination with an amorphous track structure approach. Together with the assumption of a giant-loop organization to describe the higher order chromatin structure this allows the definition of two different classes of DSB. These classes are defined by the level of clustering on a micrometer scale, i.e., "isolated DSB" (iDSB) are characterized by a single DSB in a giant loop and "clustered DSB" (cDSB) by two or more DSB in a loop. Clustered DSB are assumed to represent a more difficult challenge for the cell repair machinery compared to isolated DSB, and we thus hypothesize here that the fraction of isolated DSB can be identified with the fast component of rejoining, whereas clustered DSB are identified with the slow component of rejoining. The resulting predicted bi-exponential decay functions nicely reproduce the experimental curves of DSB rejoining over time obtained by means of gel electrophoresis elution techniques as reported by different labs, involving different cell types and a wide spectrum of radiation qualities. New experimental data are also presented aimed at investigating the effects of the same ion species accelerated at different energies. The results presented here further support the relevance of the proposed two classes of DSB as a basis for understanding cell response to ion irradiation. Importantly the density of DSB within DNA giant loops of around 2 Mbp size, i.e., on a micrometer scale, is identified as a key parameter for the description of radiation effectiveness. © 2013 by Radiation Research Society

INTRODUCTION

In the context of ionizing radiation induced DNA damage, DNA double-strand breaks (DSB) are considered as the predominant mediators of radiation-induced cell killing. However, it is obviously not only the mere number of initially induced DSB that determines the cell killing probability. Several studies suggest that residual damage, represented by a subset of DSB that cannot be quickly repaired or rejoined and persist for a longer time, is an indicator of the cell killing probability (*1–5*). This is qualitatively consistent with observations after high-LET radiation, where typically the yield of initially induced DSB is similar to that of photon radiation (*6*), but the fraction of residual damage is increased as compared to low-LET radiation, in line with the higher cell killing efficiency of high-LET radiation (*7*).

The kinetics of DSB rejoining can therefore provide important information on the biological effectiveness of different radiation qualities. After photon irradiation, typically a biphasic rejoining kinetics characterized by a fast and a slow component is adopted for the interpretation of the experimental data, although other approaches are possible (*8*). Several hypotheses have been discussed concerning the biological interpretation of these two components, and some of these suggest the presence of DNA damages of different severity, which are processed with different kinetics. This hypothesis is also in line with the slower rejoining observed after exposure to high-LET radiations compared to photons (*7, 9–11*).

The main difference between low-LET radiation (such as photons) and high-LET radiation (like accelerated ions) is that the former leads to a sparsely ionization pattern while the latter results in more dense ionization patterns. Consequently, a comparably homogeneous distribution of lesions in the volume of a typical mammalian cell is expected after photon irradiation because of the rather random spatial distribution of energy deposition events. In contrast, for ion irradiation the energy deposition is extremely localized along the trajectory of the primary ion and it can be described in terms of the average energy deposition as a function of the distance from the track center, the so called radial dose profile. The importance of

[1] Address for correspondence: GSI Helmholtzzentrum für Schwerionenforschung, Department of Biophysics, Planckstrasse 1, D-64291 Darmstadt, Germany; e-mail: m.scholz@gsi.de.

the radial dose profile becomes obvious when comparing different ion species at the same LET. Despite the same overall energy deposition, the different ion species exhibit different biological effectiveness, which can be traced back to their different track structure properties (*12–14*) indicating that LET alone is not a suitable predictor of radiation effectiveness. The different energy deposition patterns of photons and ions are reflected in the relative pattern of DNA damage and of DSB distribution in particular (*15–17*). The resulting proximity of damages induced by ion tracks is expected to lead to a higher complexity of damage, which can explain the increase of the fraction of residual damage with penetration depth for high energetic ion beams (*18*). The higher complexity of this damages can also be considered as explanation for the increased relative biological effectiveness (RBE) in the Bragg peak region, which represents one of the major rationales for application of ion beams in tumor therapy (*19–21*).

In particular for tumor therapy, an accurate quantitative description of the increased effectiveness of ion beams is required for treatment planning. The first version of the local effect model (LEM I) was originally developed for application in treatment planning with the aim to predict the RBE for cell killing and normal tissue effects of ion irradiation (*22*). The model relies on the basic assumption that the biological effectiveness of heavy-ion irradiation can be derived from the photon dose–response curve in combination with the microscopic local dose distribution pattern of ion traversals within the target (i.e., the cell nucleus). The fundamental assumption of the model is that equal local doses should lead to equal local effects independent on the radiation quality; the local dose (on a nanometer scale) is described in this context by an ''amorphous'' track structure model. Several improvements have been implemented over the years that enhance the predictive power of the model [LEM II (*23*), LEM III (*24*)] and in 2010 a new version of the LEM (LEM IV) was developed (*25*). In contrast to the previous versions, where the local dose was directly translated into an average number of lethal events, in the new version an intermediate step is introduced based on a more mechanistic description of the initial spatial DNA damage distribution.

The intermediate step involves the classification of DSB into two classes, called isolated DSB (iDSB) and clustered DSB (cDSB), respectively. In our model, isolated DSB correspond to isolated, single DSB induced in DNA domains of approximately 2 Mbp size, whereas clustered DSB are characterized by simultaneous induction of 2 or more DSB within a 2 Mbp domain.

In this current study, we test the hypothesis that these two DSB classes of isolated DSB and clustered DSB can be identified with the fast and slow rejoining components, respectively. Therefore, frequencies of isolated DSB and clustered DSB are calculated using the LEM and the corresponding rejoining kinetics is determined based on a biphasic exponential model. Rejoining after photon irradi-

ation is calculated according to the same principle. Predicted rejoining curves are then compared with experimental data for different radiation qualities and for different cell lines.

MODELING

Basics of LEM

The LEM is primarily used to simulate the biological effectiveness of cell exposure to ion irradiation in terms of clonogenic survival. In the most recent version of the model [LEM IV (*25*)], the biological response of a cell to radiation is linked to the initial DNA damage distribution inside the cell nucleus. The basic assumption behind that link is that besides the mere number of DSB it is mainly their local density that determines the cell killing probability. The DSB density is determined in the model in relationship to a key structural subunit of the chromatin organization, the so-called ''Giant Loop'' (*26, 27*). These giant loops represent DNA segments/subunits of about 2 Mbp size, whose ends are attached to the nuclear matrix. The relevance of this loop organization both from a structural and functional point of view has been also discussed in relationship to the phosphorylation of histone H2AX, which extends over a chromatin region of about 2 Mbp surrounding induced DSBs and represents a key element in the cell response to radiation damage (*28*).

The model simulates the spatial distribution of induced DSB for a given pattern of ion traversals according to the local dose deposition pattern derived from the radial dose profile of the tracks. Based on the giant loop description, individual DSB are then classified according to the number of DSB induced in individual loops. If only a single DSB is induced in a loop, it is classified as isolated DSB (iDSB); if two or more DSB are induced, they are classified as clustered DSB (cDSB). Different severities are then assigned to these two damage classes, which are assumed to be related to the probability of rejoining and repair.

When a single DSB is induced in one loop, the DNA ends are considered to be still close together and repair or rejoining processes like e.g. non-homologous end joining as well as homologous recombination should be able to reconnect the break ends with high fidelity. In contrast, when multiple DSB are induced in a loop, the production of DNA fragments inside the loop is possible and those fragments could diffuse away from the damaged site, and consequently rejoining is expected to be more difficult due to the loss of integrity of the loop structure (*29*). Following this description, clustered DSB are proposed to be more likely responsible for cell death compared to isolated DSB. This concept has been recently demonstrated to be consistent also with the general linear-quadratic shape of cell survival curves for low-LET radiation (*30*). Furthermore, the possibility that dose effects at micrometer level could influence the kinetics of DSB processing has been

TABLE 1
Physical Properties of the Radiation Qualities Employed

Ion	Energy (MeV/u)	LET (keV/μm)	Dose (Gy)	Number of independent experiments
Helium	3.7	41.0	46	1
Carbon	261.0	13.6	34	3
Carbon	186.0	16.9	38	3
Carbon	45.0	48.6	50	2
Carbon	11.0	150.3	25	3
Carbon	5.4	270.0	70	1
Oxygen	308.8	22.0	35	1
Oxygen	194.5	29.0	46	1
Oxygen	12.5	240.0	38	1
Argon	12.9	1106.0	106	2
Nickel	400.0	200.0	20	1
Nickel	12.3	2456.0	196	2
Gold	9.7	12350	138	2

TABLE 2
Input Parameters (Nucleus Radius and Domain Size) and Fitted Half-Lives for The Different Data Sets Considered

Cell line	Nucleus radius (μm)	Domain size (nm)	τ_{fast} (min)	τ_{slow} (min)
V79 Belli *et al.* (*36*)	5.0	540	14 ± 1	155 ± 6
V79 Belli *et al.* (*36*)	5.0	460	19 ± 1	215 ± 11
Human skin fibroblast (GM5758) Stenerlöw *et al.* (*37*)	8.5	540	10 ± 1	74 ± 3
Human skin fibroblast (GM5758) Stenerlöw *et al.* (*37*)	8.5	420	9 ± 1	108 ± 4
CHO-K1 Taucher-Scholz *et al.* (*35*)	5.0	540	11 ± 2	428 ± 126
CHO-K1	5.0	540	9 ± 1	220 ± 16

also recently reported by Neumaier *et al.*, together with the concept of repair centers for multiple DSB induced in close vicinity (*31*).

Calculation of Isolated DSB and Clustered DSB

For each simulation both the cell line and the radiation quality have to be appropriately characterized, and each cell line, the following parameters are used to define the target features:

1. Cell nuclear volume and radius.
2. Length of DNA segments representing a giant loop.

The cell nucleus is defined as a cylinder with the main axis parallel to the ion direction. A constant volume of 500 μm³ is assumed for all cell lines; the geometry is then defined by the particular choice of the nuclear radius, from which the corresponding height is determined. The total DNA content is fixed and equal to 5.4×10^9 bp. Concerning the cell lines investigated here, some differences can be expected in the total amount of DNA content, with some slightly higher values characterizing human cell lines. The effect of a 10% increase of DNA for human fibroblast has been tested (data not shown), and no significant differences were observed in the final outcome. This is probably due to the fact that for the analysis presented here we focus on the relative fraction of isolated DSB and clustered DSB, but not directly on their absolute numbers. The giant loop structure is actually represented by cubic shaped domains of fixed size inside the cell nucleus, assuming that a volume can be uniquely assigned to a given length of a DNA segment if the DNA is homogenously distributed throughout the cell nucleus. A standard value of 540 nm has been used in the LEM as the edge length of the cubical domains, which has been derived from an optimization procedure used to minimize the deviations between model predictions and experimental data sets (*25*). This value is fully in line with values

found in the literature (*26, 27*). Nevertheless, since the relative fractions of isolated DSB and clustered DSB critically depend on the domain size, we further analyzed the impact of this parameter by varying it with a step size of 40 nm between the extreme values of 540 nm and 420 nm. This range corresponds to a genome content per domain from around 2 Mbp down to around 500 kbp of DNA respectively. The domain size, as well as the radius of the cell nucleus, determines the number of giant loop domains that are contained inside the nucleus. The parameter values for the cell lines of interest are summarized in Table 2.

Concerning radiation quality, any ion species can be simulated by selecting the appropriate combination of energy, LET and physical dose value. No modifications have been made on the description of the track structure and the calculation of the initial DSB distribution, which have been extensively described in previous works (*23, 25, 29*).

The LEM complete simulation algorithm (*29*) was used to perform all the simulations of DSB distribution patterns, neglecting in this context the further step involving calculations of cell survival probabilities. The numerical values obtained as output from one single simulation, are used to evaluate a mean number of domains containing isolated DSB, n_i, and a mean number of domains containing clustered DSB, n_c, for each particular irradiation, assuming Poissonian statistics for the random ion hits on the cell nucleus. The total number of DSB corresponds to the sum

$$n_{DSB} = n_i + n_c \cdot \lambda_c$$

where λ_c represents the mean number of DSB per clustered DSB.

Concerning photon irradiation, the Poisson distribution is adopted to describe the random distribution of DSB inside

the cell nucleus (*32*), which for each cell line is characterized as already described. Assuming a Poisson distribution, and with N_L defining the number of loops available inside the nucleus and D the released dose, we can calculate the number of domains affected by isolated DSB and clustered DSB, respectively (*29, 30*):

$$n_i(D) = N_L \lambda(D) e^{-\lambda(D)}$$

$$n_c(D) = N_L(1 - e^{-\lambda(D)} - \lambda(D) e^{-\lambda(D)}) \quad (1)$$

The average number of DSB per domain $\lambda(D)$, defined as follows, depends on the DSB yield α_{DSB}, on the dose and on the total number of domains:

$$\lambda(D) = \frac{\alpha_{DSB} D}{N_L} \quad (2)$$

As for the simulations of ion radiation, α_{DSB} is chosen equal to 30 DSB per Gy and cell nucleus (*33, 34*).

Rejoining Model

Based on the total number of DSB and the corresponding frequencies of isolated DSB and clustered DSB, the relative fractions of isolated DSB and clustered DSB can be determined. The main hypothesis made here is that according to the severity of damage, as discussed above, isolated DSB are assumed to be rejoined with a fast kinetics, whereas DSB contained in clustered DSB are assumed to be rejoined with a slow kinetics. Although it cannot be excluded that differences in damage severity are connected to the actual number of DSB induced in a loop, we restrict ourselves here to a distinction between domains affected by only one, or by two or by more than two DSB. This is based on the assumption that the main difference from the point of view of the repair processes lies in the integrity of the loop structure, which is maintained only in the case of isolated DSB.

The fractions F_{fast} and F_{slow} corresponding to the weights of the two damage classes in the kinetic curves are thus defined as follows:

$$F_{fast} = \frac{n_i}{n_i + n_c \cdot \lambda_c}$$

$$F_{slow} = \frac{n_c \cdot \lambda_c}{n_i + n_c \cdot \lambda_c}$$

$$\lambda_c = \frac{n_{DSB} - n_i}{n_C} \quad (3)$$

where n_i and n_c indicate the number of domains affected by isolated and clustered DSB respectively, n_{DSB} represents the total number of DSB and λ_c refers to the mean number of DSB per cluster. The DSB rejoining over time after irradiation and the fraction of unrejoined DSB at time t, U(t), can be calculated as a biphasic exponential decay of

the fast and slow components, characterized by the half-lives τ_{fast} and $\tau_{slow,}$ respectively:

$$U(t) = F_{fast} e^{-\frac{\ln(2)}{\tau_{fast}}t} + F_{slow} e^{-\frac{\ln(2)}{\tau_{slow}}t} \quad (4)$$

According to Eq. (4) the induced DNA damage is normalized to 1 at t = 0, before decreasing over time with two different rejoining kinetics.

In accordance with the general concept of the LEM, we assume that for a given cell line the short and long half-lives, attributed to isolated DSB and clustered DSB, respectively, do not change depending on whether the isolated DSB and the clustered DSB were induced by photon or high-LET irradiation. The different rejoining kinetics can then be fully attributed to the different relative fractions of isolated DSB and clustered DSB, translating into different relative fractions of fast and slow components. Consequently, we determine the corresponding half-lives by fitting Eq. (4) simultaneously to the low-LET and high-LET data for a given data set. The fit is based on a χ^2 minimization on a linear scale and error bars are considered. The resulting half-lives are summarized in Table 2.

Experimental Data Sets for Comparison

The data chosen for comparison were obtained by using different radiation qualities and cell lines. Photons as well as a wide spectrum of ions have been considered, ranging from light ions (proton, deuteron, helium), up to intermediate (carbon, nitrogen, oxygen, neon) and very heavy ions (argon, nickel, xenon, gold). The cell lines involved in the mentioned experiments were V79, CHO-K1 and human skin fibroblast (GM5758). Some experimental data are also taken from published data sets (*35–37*). However, for further validation of the model over a wide range of ions and LET an additional large set of new experimental data on DSB rejoining is also included. These experimental data were produced with the aim of specifically investigating the effect of the same ion species at different energies. Typical doses of gel electrophoresis experiments in the range of 20–200 Gy were applied. The information concerning the different radiation qualities employed to perform the experiments are summarized in Table 1. Due to limited access to the irradiation facility, part of the experiments was performed only once. The information concerning the number of available independent experiments for each radiation quality is reported in Table 1. The new rejoining measurements were carried out as described previously (*6*). Briefly, plateau phase cells (CHO-K1) were irradiated in monolayers at the UNILAC accelerator at GSI (low-energy ions) and embedded in agarose plugs after repair incubation under culture conditions. Alternatively, for X rays or high-energy-ion irradiation, the cells were directly embedded in agarose plugs, then irradiated and kept under culture conditions during repair. Cell lysis was done in plugs incubated in Proteinase K lysis buffer at 50°C for 20 h. Plug pieces containing around 10^5 cells were loaded on 0.5%
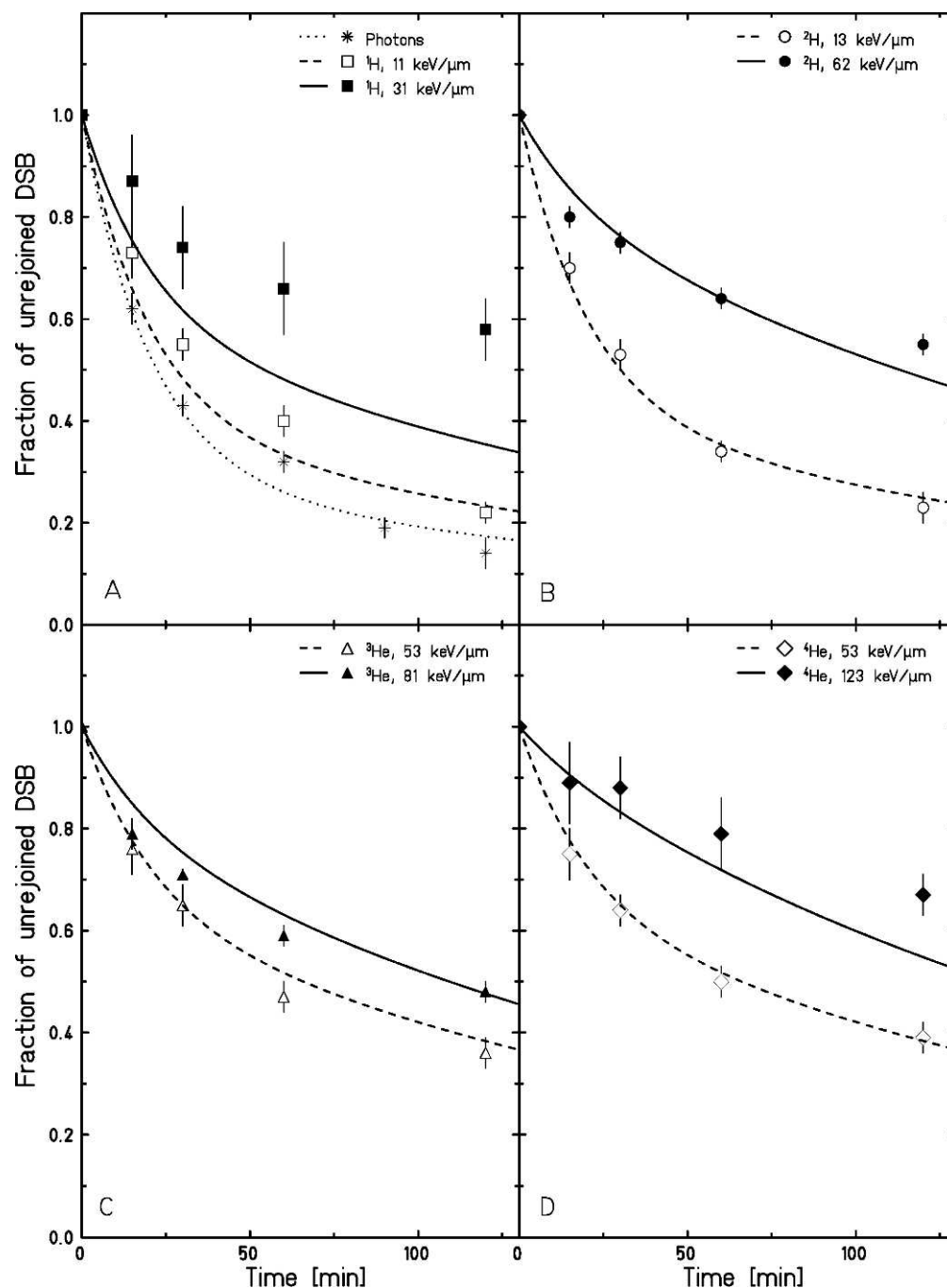
FIG. 1. Experimental data of DSB rejoining over time after irradiation of V79 cells with photons and protons (panel A), deuterons (panel B), helium-3 ions (panel C) and helium-4 ions (panel D) as reported by Belli *et al.* (*36*) (symbols) and corresponding model predictions (lines) based on a domain size of 540 nm. The absorbed dose was 45 Gy for all radiation qualities.

agarose gels and subjected to constant field gel electrophoresis at 1 V/cm for 20 h. The fraction of eluted DNA was quantified based on the fluorescence intensity measurement after ethidium bromide staining.

Due to experimental limitations not all the fragments produced by the incident radiation can be measured with this technique, but usually an upper limit of around 6 Mbp and a lower limit of few kbp can be considered to define the

range inside which the measurement can be performed (*36–38*). In addition only the physical rejoining of fragments can be measured by this procedure, but nothing is known concerning the accuracy of the rejoining and the resulting biological effects. In some cases at very low energies, track segment conditions were not fulfilled anymore because of the small residual energy and thus correspondingly short range of the ions. This can lead to a significant variation of
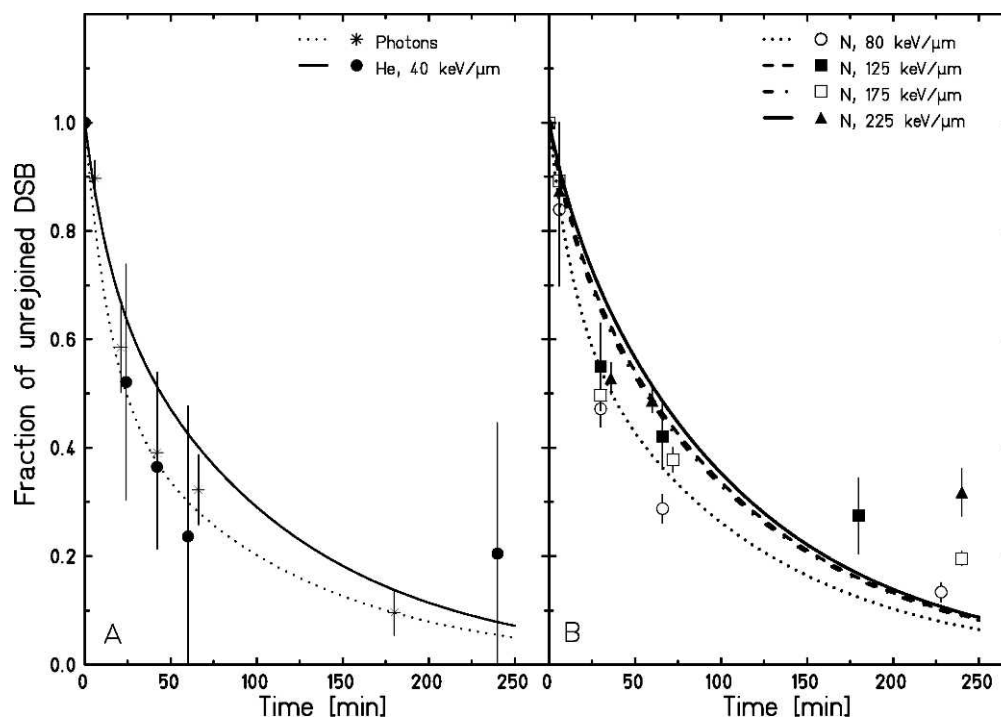
FIG. 2. Experimental data of DSB rejoining over time after irradiation of human skin fibroblast cells with photons and helium ions (panel A) and nitrogen ions (panel B) as reported by Stenerlöw *et al.* (*37*) (symbols) and corresponding model predictions (lines) based on a domain size of 540 nm. The physical dose was 100 Gy for all radiation qualities.

LET along the path of a particle traversing the cell nucleus. Furthermore, it has been described that the cell lysis at high temperature, which is part of the experimental protocol, is responsible for the conversion into DSB of the so-called heat-labile sites induced by radiation (*39*), meaning that a fraction of the measured DSB could represent an experimental artifact these aspects will be further considered during the discussion of the results.

RESULTS

Full Rejoining Curves

In Fig. 1, predictions of the rejoining model are compared to experimental results as reported by Belli *et al.* (*36*) after irradiation of V79 cells with photons, protons, deuterons and helium ions at a dose level of 45 Gy. For the simulations, deuterons are treated as protons at the same LET. As clearly visible from Fig. 1, there is good agreement between the model and experimental data for photons in the whole range taken into consideration, and the rejoining after ion irradiation seems to be reasonably well reproduced, although some deviations are observed which affect in particular the highest LET and the latest time points for protons (Fig. 1A) and helium-4 (Fig. 1D). In this case an underestimation of the residual damage is observed with the model, while the fast component of the rejoining seems to be well reproduced. It should be noted that for each ion the highest LET corresponds to a residual range for the particle

that is comparable to the thickness of the cell layer. Consequently, a significant increase of LET could take place during the traversal of the cell layer, which is not taken into account by the model and could explain the observed underestimation.

Figure 2 compares model predictions with experimental data obtained after irradiation of human skin fibroblasts irradiated with 100 Gy of photons, helium and nitrogen ions at different energies as reported by Stenerlöw *et al.* (*37*). Again a reasonable agreement is observed for photons, while more pronounced deviations of the model predictions from experimental results are observed in the case of high-LET radiation (Fig. 2B). Whereas the slope of the slow component of rejoining is relatively well reproduced, at least for the lowest LET, a general underestimation of the rejoining capacity is registered in the first hour, followed by an overestimation of rejoining at the latest time points. Moreover, the differences in the rejoining kinetics observed in experimental data for different LETs are larger than the ones obtained with the simulated rejoining.

To analyze the impact of the specific choice of the parameter characterizing the loop/domain size, we repeated the analysis shown in Figs. 1 and 2 using different values for the domain size. Obviously, the choice of a different size for the domains results in a different number of domains for a given volume of the nucleus (fixed to 500 μm^3), and consequently in different fractions of isolated DSB and clustered DSB. The optimal values were determined by the
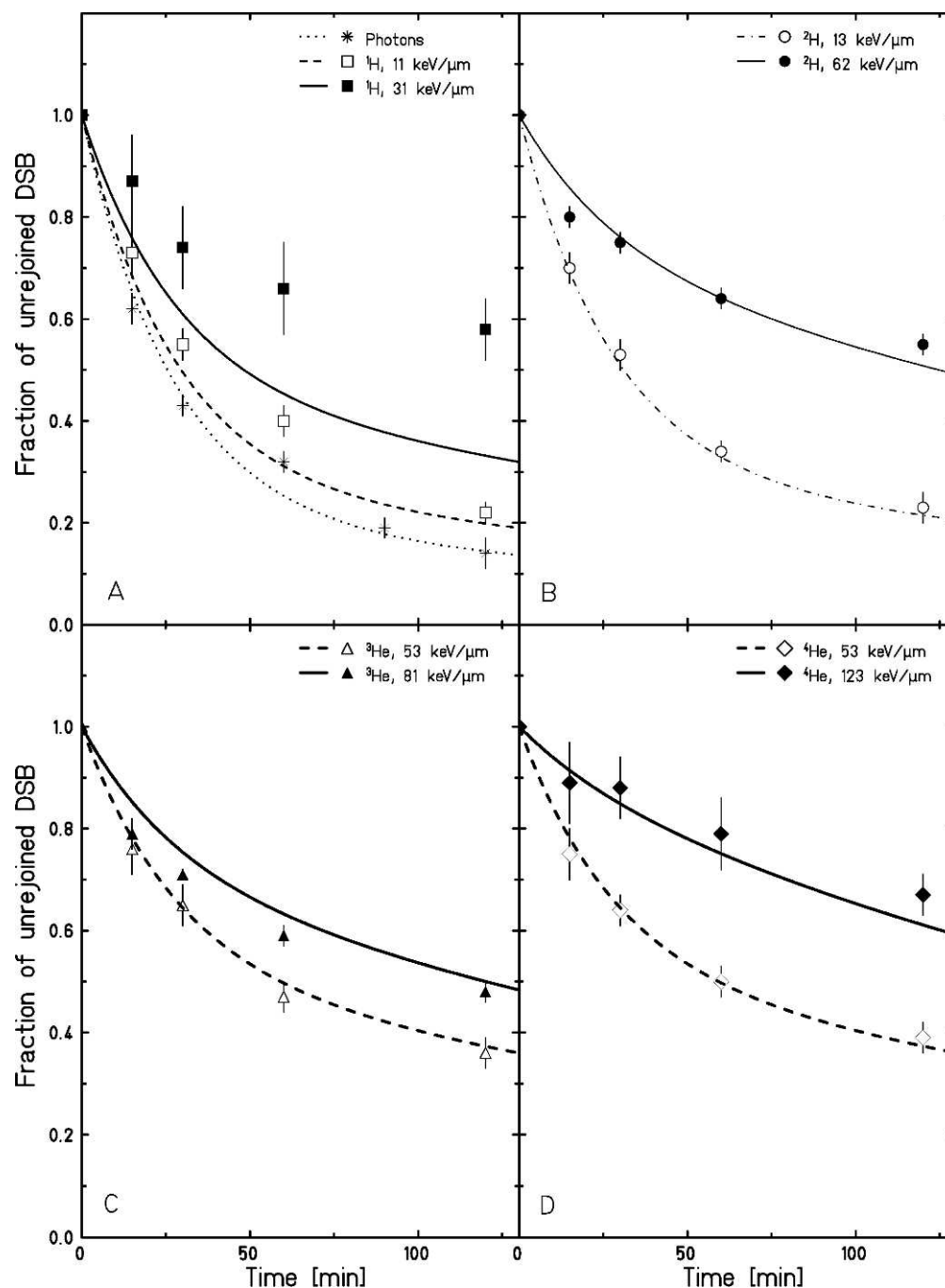
FIG. 3. Experimental data of DSB rejoining over time after irradiation of V79 cells with photons and protons (panel A), deuterons (panel B), helium-3 ions (panel C) and helium-4 ions (panel D) as reported by Belli *et al.* (*36*) (symbols) and corresponding model predictions (lines) based on a domain size of 460 nm. The absorbed dose was 45 Gy for all radiation qualities.

lowest χ^2 resulting from the fit procedure when the parameter is reduced from 540 nm down to 420 nm in 40 nm steps. The length of 460 nm corresponds to sub-volumes involving about 1 Mbp of DNA, while with 420 nm we have about 700 kbp of DNA per giant loop for the two cell lines. Both the values are within the size range, which is under current discussion (*40–43*).

As shown in Figs. 3 and 4, an improvement in the comparison with experimental data is obtained by reducing the domain size to 460 nm for V79 cells and to 420 nm for human skin fibroblast. Concerning the V79 cells, results calculated for a reduced domain size are reported in Fig. 3. Again good agreement is obtained for photon data, and some improvements are observed with ions too (Fig. 3A and
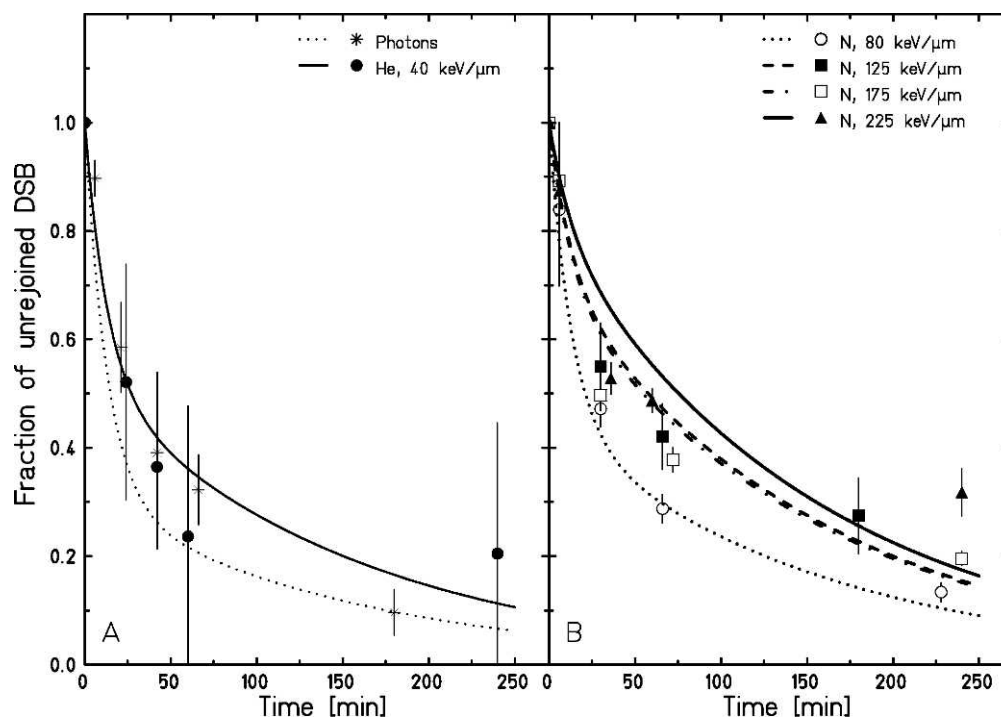
FIG. 4. Experimental data of DSB rejoining over time after irradiation of V79 cells with photons and protons (panel A), deuterons (panel B), helium-3 ions (panel C) and helium-4 ions (panel D) as reported by Belli *et al.* (*36*) (symbols) and corresponding model predictions (lines) based on a domain size of 420 nm. The absorbed dose was 45 Gy for all radiation qualities.

D), compared to the results obtained with a domain size of 540 nm. Deviations are now smaller, but the consideration already made for the short range of the high-LET particles still has to be considered. The adjustment of the domain size seems to more greatly affect the modeling of the human skin fibroblast data. By reducing the domain size to 420 nm (Fig.
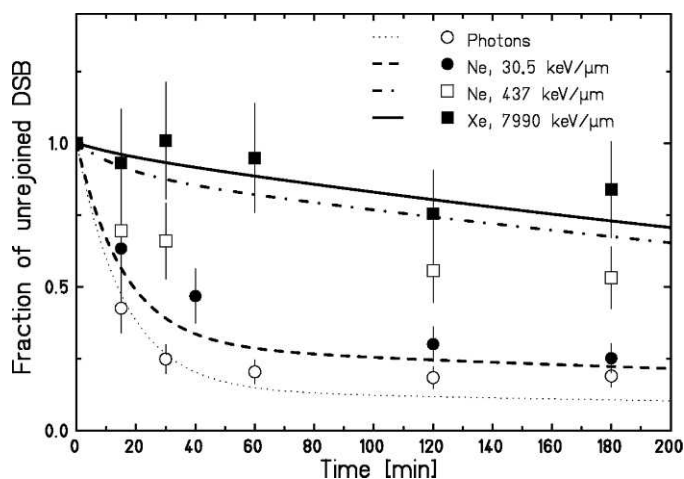

FIG. 5. Experimental data of DSB rejoining over time after irradiation of CHO-K1 cells with xenon ions (77 Gy), neon ions (38 Gy and 13 Gy for 30.5 keV/μm and 437.0 keV/μm, respectively) and X-rays (20 Gy) as reported by Taucher-Scholz *et al.* (*35*) (symbols) and corresponding model predictions (lines) based on a domain size of 540 nm.

4) the agreement for the fibroblast photon experimental data as well as the ion data is significantly improved compared to the standard dimension of 540 nm (Fig. 2). Even though full agreement of the model and the data is still not yet obtained, as a consequence of a reduced domain size we observe a more accurate description of the fast component, which is the result of the smaller fraction of induced clustered DSB. In addition, the residual damage at the latest time points now deviates less from the experimental data, and the general variation of the rejoining patterns with LET as predicted by the model is closer to the experimentally observed variation in comparison to the standard settings (Fig. 4B). We therefore conclude that for this specific fibroblast cell line, a smaller dimension of the domain seems to result in a more realistic description of the relative proportion of induced isolated DSB and clustered DSB for photon as well as for ion irradiation.

We then further tested the model by investigating even heavier ions and higher LET values. In Fig. 5, the model is used to predict the DSB rejoining for CHO-K1 cells after irradiation with photons, neon and xenon ions (*35*). The LET for ion irradiation ranges from 30.5–7,990 keV/μm. Since no error bars were reported for this data set, a 20% error was assumed for the single points in agreement with the quality of the measurements as discussed by the original authors (*35*). This value is also in line with the experimental error calculated for similar repeated experiments involving gel electrophoresis elution techniques. When comparing
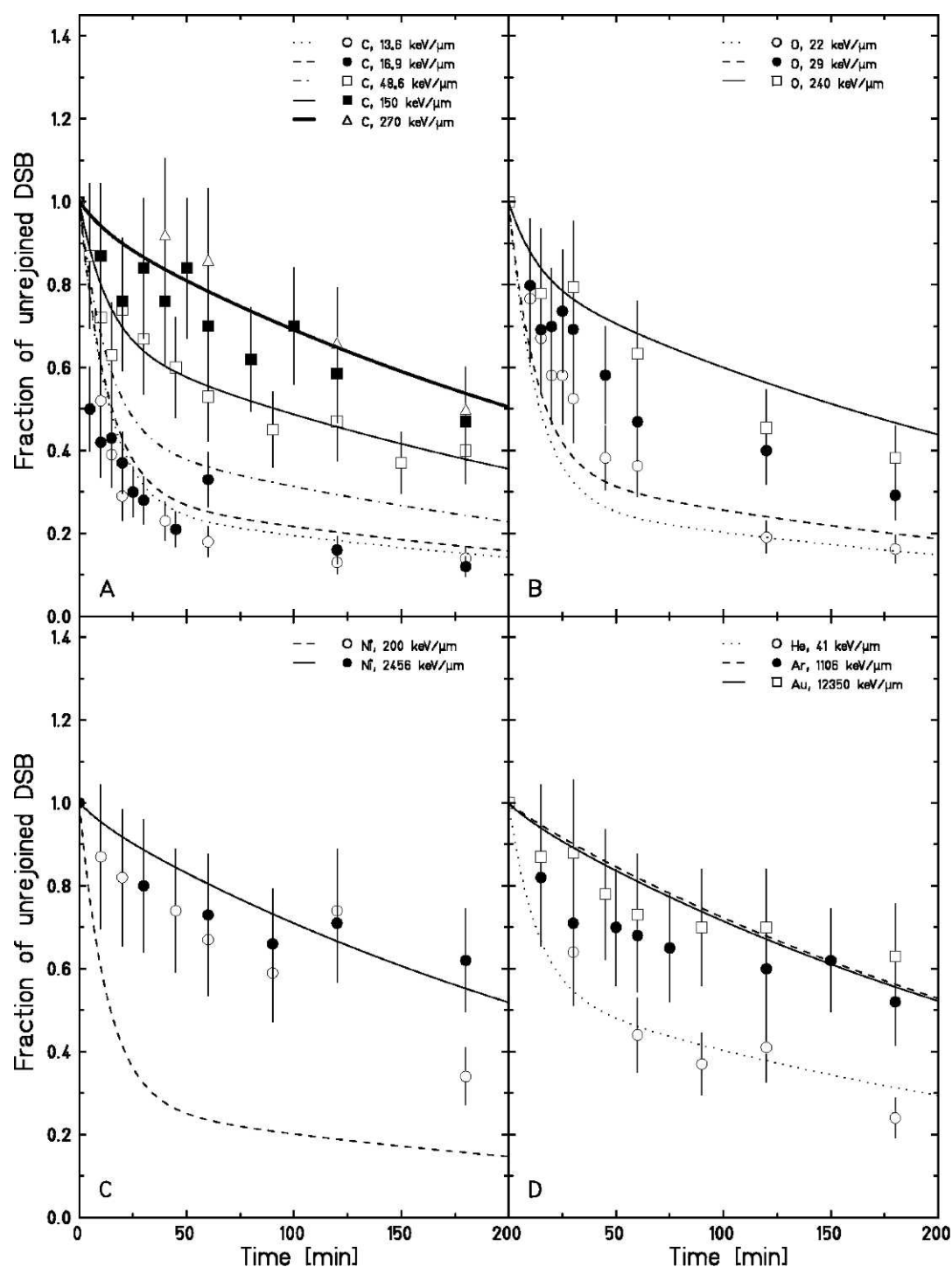
FIG. 6. Experimental data (symbols) and corresponding model predictions (lines) of DSB rejoining over time after irradiation of CHO-K1 cells with carbon ions (panel A), oxygen ions (panel B), nickel ions (panel C), helium, argon and gold ions (panel D). The model is used here with a domain size of 540 nm. The corresponding dose values are provided in Table 1.

experimental data and model predictions, a very good agreement is obtained for the extreme cases of photon and xenon irradiation. The high LET of xenon ion results in a fraction of clustered damage representing more than 95% of induced damage, which is then reflected in the predicted rejoining curve being dominated by the slow component.

For neon irradiation, the experimental data are well reproduced for the lower LET, while deviations are observed for the higher one. At the higher LET neon irradiation a pronounced fast component can be observed in the experimental rejoining, which is not reproduced by the model, although the slope of the slow component seems to
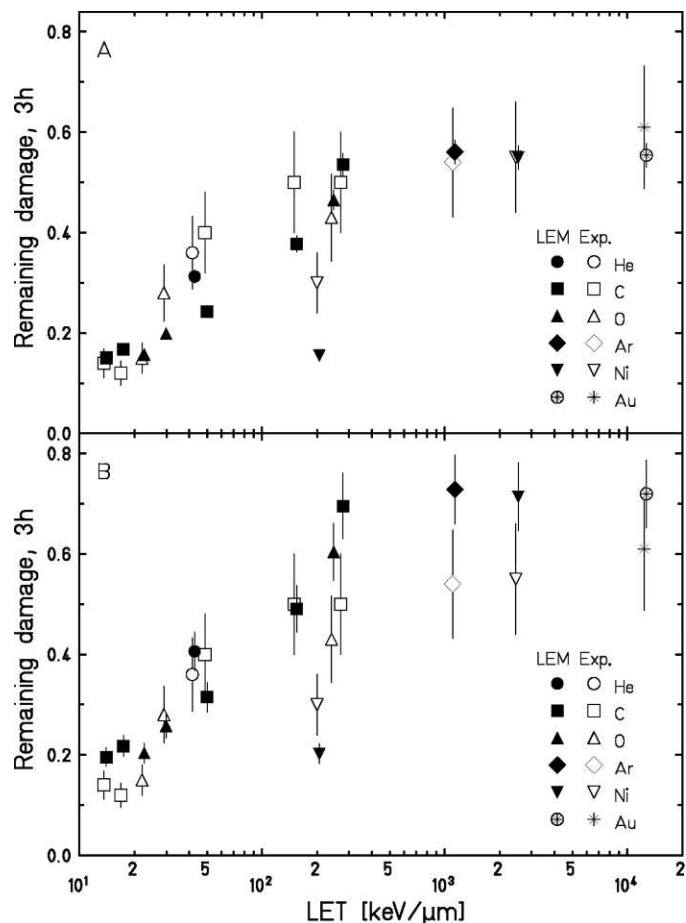
FIG. 7. Experimental data (open symbols) and corresponding modeling results (closed symbols) of the remaining fraction of DSB 3 h after photon and ion irradiation of CHO-K1 cells; panel A the remaining fractions of unrejoined breaks are calculated by using the half-lives resulting from the fits of Fig. 6, while in panel B they are predicted by adopting the half-lives resulting from the fits of Fig. 5. Symbols referring to experimental and modeling results at the same LET are slightly shifted to allow a clear visualization of the error bars. The model is used here with a domain size of 540 nm. The corresponding dose values are provided in Table 1.

be comparable. The result is a general underestimation of DSB rejoining in this time window. The effect of a variation in the domain size was investigated; however, no improvement has been achieved in this case (data not shown), and the standard value of 540 nm gives the best results.

Figure 6 shows the application of the LEM model to a new set of experimental data produced in our laboratory after irradiation of CHO-K1 cells with different ion species covering a large-LET spectrum from 13.6 keV/μm carbon ions up to 12,350 keV/μm gold ions (detailed physical parameters are reported in Table 1). Error bars were set to 20% of each data point as discussed above. In most cases, nice agreement was observed. To investigate the effect of the same ion species accelerated at different energies, i.e., carbon ion (Fig. 6A), the large-LET range covered by the experiments (from 13.6 to 270.0 keV/μm) allowed visual-

ization of a gradual transition of the DNA damage pattern from a photon-like condition at the lowest LET values, with isolated DSB representing the majority of the induced breaks, to an intermediate one where isolated DSB and clustered DSB are distributed in similar fractions, up to the highest LET showing a dominating slow component of rejoining. When looking at single curves, we can again observe a good agreement for the extreme-LET values, while the predicted rejoining shows some deviations from the experimental data in the intermediate-LET range, going in the direction of a general overestimation of fragment rejoining, even though the slope of the slow component appears to be nicely reproduced. When extending these considerations to the other ion species, the same trend is observed, with a good agreement in the case of low and high LET and some larger deviations in the intermediate range. Only for nickel ions at 200 keV/μm does the model fail to describe the full rejoining curve (Fig. 6C). We note in particular the lack of a fast component in the experimental results, whereas the model predicts such a fast component. Therefore the deviations are pronounced in the first hour and get progressively smaller at later time points. As for the previous data set, the effect of a variation of the domain size was considered (data not shown), but the best agreement to measured data again was obtained with the standard value of 540 nm length. Together with the previous analysis, this result indicates that the standard domain size is optimal for this particular cell line.

LET Dependence of Remaining DSB Fraction after 3 Hours

In Fig. 7A we show the remaining fraction of DSB at 3 h after irradiation as function of the LET for the same radiation qualities considered in Fig. 6. Experimental data were extracted from the full rejoining curves, while the simulated values were calculated by combining the initial DSB distribution patterns predicted by the LEM with the half-lives resulting from the fits shown in Fig. 6. The error bars associated to simulated values reflect the uncertainty in the fitted half-lives (Table 2). In most of the cases good agreement is obtained between experimental and simulated rejoining, despite some deviations that are observed for the carbon ions in the intermediate-LET range, as already visible in Fig. 6. From a general point of view, it is important to note that the simulations can reproduce the increase in the fraction of remaining damage with increasing LET. Furthermore, a saturation-like behavior in the rejoining process is observed starting from a LET value of around 200 keV/μm both in experiment data and in simulations. In some cases, different ion species are investigated at similar LET, as for example carbon and nickel at approx. 200 keV/μm. Looking at the 3 h time point after irradiation, allows demonstration of the influence of the track structure on the induced DSB pattern. Since nickel ions have a much higher charge compared to carbon ions at a given LET, they are characterized by a higher specific

energy and thus a larger track radius. According to the parameterization used in the model calculations, the maximum radius of such a carbon ion track corresponds to 3.6 μm, while for nickel ion it is about 3,300 μm. Consequently, for carbon ions due to their smaller track radius and the resulting higher ionization density, we would expect a higher level of clustering, while for the nickel the same LET is spread over a much larger region reflected in a photon-like pattern of energy release. Keeping in mind that the experimental data for nickel at 200 keV/μm tend to underestimate the fast component of rejoining in comparison to the other experimental data, the remaining damage at 3 h could be expected to be even somewhat lower in that case. Overall the experimental data as well as the model outcomes support the expectations based on track structure.

We then tested the predictive power of the model by using only a limited set of data for the derivation of the half-lives. In Fig. 7B we applied the half-lives determined from the fits to the already published data for CHO-K1 cells as shown in Fig. 5 to predict the remaining damage at 3 h for all ion-energy combinations of the new experimental data as shown in Fig. 6. It is interesting to see that even when using the half-lives obtained from the fit of Fig. 5 to predict the fraction of remaining damage an overall good agreement is obtained. However, in this case slightly different systematic deviations are observed. Whereas now reasonable agreement is found in the low- and intermediate-LET regions, the systematic deviations are more pronounced in the high-LET region. In general, somewhat larger deviations can be expected compared to the case shown in Fig. 7A because of the far more limited set of data used to derive the relevant parameters. Nevertheless, Fig. 7B nicely demonstrates the predictive power of the model, since even based on the limited data set of Fig. 5 the model is able to reproduce the general features of the remaining damage as a function of radiation quality reasonably well.

DISCUSSION

In this investigation the LEM model has been used for the first time as a tool to describe the DSB rejoining over time after ion irradiation, whereas originally the model was developed for different purposes, namely to predict the increased effectiveness for cell killing. The aim of the analysis presented here was to specifically test the significance of the two damage classes introduced in the LEM, i.e., isolated DSB and clustered DSB. We hypothesized that the classes of isolated DSB and clustered DSB could be attributed to the fast and slow components of rejoining, respectively. By combining the patterns of DSB distributions obtained with the LEM and a simple biphasic exponential rejoining kinetics, the model is able to reasonably predict the DSB rejoining over time for three different cell lines and several different radiation qualities. The agreement obtained in the comparison further supports

the new mechanistic approach on which the LEM is currently based.

In particular cases, significant deviations are observed between experimental and simulated data, however, these deviations do not follow a clear systematic trend and they can be partially explained by variations in experimental procedures, biological factors and modeling features, which will be discussed below.

Nevertheless it must be kept in mind that the actual application of the LEM exceeds the aim for which it was originally developed. In that respect, it is of interest to note that with increasing LET, the model is able to predict the saturation in the rejoining process at very high LET values as observed in the experiments (Fig. 7). In the context of our model, this is due to the progressively enhanced fraction of clustered DSB, which finally translates in only a single component, namely the slow one, being relevant for the description of the DSB rejoining over time. It will therefore be interesting to investigate in more detail how directly the saturation in the rejoining process at high LET relates to the enhanced RBE of ion irradiation in the Bragg peak region as predicted by the LEM.

Influence of Experimental Limitations

In the gel electrophoresis elution technique, it is impossible to measure all the DNA fragments produced by irradiation. For practical reasons, the measurements involve a defined range of fragment lengths, which usually has about 6 Mbp as upper limit and few kbp as lower one (*36–38*). This happens because fragments larger than 6 Mbp are too large to migrate into the gel, while fragments below about 5 kbp are short enough to migrate out of the gel. Both classes of fragments are therefore excluded from the measurements. According to dedicated studies (*44, 45*) with ion irradiation an increased number of small fragments are produced compared to photon exposure, and at increasing LET a significant percentage of fragments has a length below the measurable limit, consequently affecting the accuracy of the measurements. By contrast, really large fragments represent only a minor fraction of the total number and can be neglected from the discussion since they are not expected to greatly affect the final results. The above experimental limits are reflected in the context of our analysis, since at the actual stage all the induced fragments are taken into account in our model. Focusing on the small fragments, they should represent DSB induced in close proximity, which are considered as clustered DSB in the picture described by our model. This consideration could help to explain some of the deviations observed in the comparison: when the model predicts an overestimation of the residual damage or an underestimated fast component, this could be due to the loss of short fragments during the experiment, resulting in an experimental underestimation of the slow component of induced damage.

As already mentioned above, it has been demonstrated that DSB measurements using gel electrophoretic elution techniques are affected by the conversion of the so-called radiation induced heat-labile sites into DSB when the lysis is performed at high temperatures (*39*). More recently, it was shown that this effect reflects at least in part a biological process also taking place during incubation at physiological temperatures (*46*). Furthermore, it seems to be less relevant after high-LET irradiation and a cell line dependence was also reported (*34, 46*). Considering these various aspects and despite the fact that corrections factors have been proposed to take into account this potential artefact low LET (*47*), in our view these minor effects (especially for high LET), that do not require more detailed consideration in the model and would not affect the final picture resulting from our study.

More generally speaking, small deviations in the comparison could be also due to uncertainties in the measurements of dose, which are usually in the order of 10% (*48*).

Impact of the Domain Size

As clearly evident from the results shown in the previous sections, the domain size is a relevant parameter to describe the cell behavior after irradiation, since it affects the proportions of induced isolated DSB and clustered DSB. Up to now a standard domain size of 540 nm length has been used in the LEM, but adjustments of this parameter are reasonable when the aim is to describe the response of different cell types. The effect of a variation of the domain size in the range 420–540 nm was investigated and showed that in some cases a reduced size better represented the data of specific cell lines (460 nm for V79, 420 nm for human skin fibroblasts). The size range chosen here approximately reflects the bandwidth of domain sizes reported by Johnston *et al.* (*41*), covering sizes of about 1–2 Mbp for different cell lines. The present analysis should be only interpreted in terms of the impact of the assumed domain sizes on our analysis. A full, detailed analysis of the influence of this parameter on the LEM predictions is beyond the scope of this work. Nevertheless, the results presented here demonstrate that improvements can be obtained in the model by adopting specific domain sizes for individual cell lines. However, if one considers that a single domain should represent one giant loop of the higher order chromatin structure, it is clear that the choice of a constant value to describe all the domains is probably not realistic from a biological point of view but is a good approximation for the first stage analysis. A more accurate and realistic description of the chromatin structure could probably be obtained by simulating a distribution of domain sizes around a mean value. This aspect is currently under investigation in our group, and could be the object of further improvements of the model.

Selection of Time Window

When selecting the experimental data sets for our analysis, we decided to restrict the application of the model to the first few hours after irradiation. One reason for this decision was the higher accuracy of the method in the measurement of fragments in the first hours compared to very late time points. Moreover, a time window of 3–4 h after irradiation allows for sensitivity to both the fast and slow component of rejoining. In contrast, the experimental data at very late time points (24 h or more) still show the presence of residual DSB. These residual DSB can be considered as a minor fraction of the induced lesions, which have not yet been processed, although at least for low-LET radiation some late rejoining can be observed up to 72 h. The presence of this plateau-like behavior at late times is not taken into account in our model, and consideration of this aspect would need the introduction of additional free parameters.

Damage Complexity Versus Chromatin Structure

Apart from giving a partial validation to the LEM model, the reported results also enhance the confidence in the proposed two classes of DSB and more generally in the clustering of DSB at a micrometer level, as being relevant for the description of cell killing after ion irradiation. Several possible classifications for the different types of DNA damage clusters have been proposed over the years to describe the increased RBE observed after ion irradiation. However, it is not yet clear whether clustering on a length scale of up to a few 10 bp or clustering on a substantially larger scale determines radiation effectiveness. For example, the work reported by Sutherland *et al.* (*49*), as well as the modeling work done by Nikjoo *et al.* (*50*) and by Ottolenghi *et al.* (*51*), supports the role of very short scale clustering, or ''locally multiple damaged sites'' as defined by Ward (*52*). Conversely, recent experimental evidence also reported the importance of clustered DNA damage on a larger scale for the understanding of the biological effects of high-LET radiation (*53*). Furthermore, a deviation from a random distribution of DNA fragments has been demonstrated by several authors when analyzing fragment size distributions a few hours after irradiation, indicating an excess presence of DNA fragments on a length scale between a few kbp to 2–3 Mbp. This observation has been associated with the presence of a higher order chromatin structure involving elements of micrometer size and to the difficulty to rejoin multiple lesions inside a single structural element (*54, 55*). These conclusions are in line with earlier work reported by Johnston *et al.* (*56, 57*), in which higher order chromatin structure defined as Mbp loops are shown to be relevant for the description of the severity of DNA damage after irradiation and refer in particular to the prolonged existence of such DSBs induced as multiple lesions in the same loop. Further support for these conclusions comes from modeling work reported by Friedland *et al.* (*58*), where a better correlation to the cell

inactivation experimental data was found for DNA damage clustering at a regional scale compared to the local scale. It therefore can thus not be excluded that, depending on the particular assay, endpoint and radiation quality, clustering on both levels might be relevant to characterize the biological effectiveness of a specific radiation quality. In that respect it is of interest to note that our model actually takes into account clustering at both levels, since besides the DSB + DSB clustering on the level of giant loops for the calculation of the initial yield of DSB, the potential combination of two SSB produced in close neighborhood is also considered as a source for an increased yield of DSB (23).

Another possible interpretation of the biphasic rejoining is that the fast component of DSB repair is induced in the euchromatic regions of the cell nucleus and the slow component of DSB repair is produced in the heterochromatic regions, as has been demonstrated for low-LET-induced DNA damage (59). However the experimental immunostaining-based techniques usually employed to investigate this endpoint require the use of different dose levels, and to measure the slow component of repair requires the assessment at later time, resulting in data which are not directly comparable to data obtained by gel electrophoresis elution techniques (60). Furthermore, it has been recently shown that the slower repair of DSB after ion irradiation, is due to the higher complexity of the induced damage and in addition the chromatin organization needs to be considered (11). Currently different levels of chromatin condensation are not taken into account in our model.

Comparison to Other Models

In the literature other models can be found for the description of DSB rejoining after irradiation and here we will briefly discuss some of them. In the stochastic model of DNA fragment rejoining recently published by Li *et al.* (61) a biochemical approach is adopted to describe the impaired fragment rejoining and the increased efficiency in the induction of cell death and mutations resulting from ion irradiation. Starting from the experimental findings concerning an enhanced production of small DNA fragments subsequent to high LET as compared to photon radiation, the hypothesis is made that protein recruitment is hindered at the break sites for very small fragments. This could result in a slow rejoining kinetics and a residual fraction of fragments that remain unrejoined. The model was applied to experimental data from radiation induced foci kinetics after irradiation with photons and 150 keV/μm Fe ions.

A numerical-analytical approach has been used by Pinto *et al*. (62) with the aim of describing the initial DNA fragmentation and rejoining kinetics induced by different radiation qualities. Pinto and others developed a new model of DNA breakage where the initial DNA damage distribution is simulated using a clustered breakage approach (62). Particular emphasis was focused on the evaluation of the so-

called background DNA damage that could result from experimental techniques. The model was applied to reproduce experimental data obtained by means of gel elution techniques after X-ray and α-particle irradiation. The authors concluded that the delayed rejoining observed after high-LET irradiation resulted from an enhanced lesion complexity at the nanometer scale (63).

The PARTRAC (PARticle TRACks) code (64) has been recently complemented by a new module for the description of DNA repair through the NHEJ pathway (65). This Monte Carlo based modeling tool has been used for the description of DSB induction and rejoining after photon and ion irradiation (66), using experimental data obtained by means of gel elution techniques. The main feature of the model from a biological point of view is the ability to reproduce DNA fragments distributions both at the initial stage and during time points when repair is ongoing. Comparison with experimental data are reported in this article for ^{60}Co γ rays and N ions of 80, 175 and 225 keV/μm.

A detailed and more direct comparison to the above mentioned models is beyond the limits of this work, and could be discussed in future publications. Nevertheless, the different approaches adopted in the mentioned models show some similarities and some differences with the LEM model we presented here. Although they are able to consistently reproduce experimental curves, the other models require a larger number of assumptions and free parameters compared to the model we proposed. Moreover, in the analysis we have presented here, successfully applied are joining model to a very wide spectrum of experimental data coming from different labs and involving different cell lines and radiation qualities.

CONCLUSION

We have demonstrated that for a given cell line a single set of biological parameters in our model is able to simultaneously reproduce the biphasic DNA rejoining kinetics over a wide range of radiation qualities. The present results combined with previous ones investigating the RBE for cell survival (25, 29) strongly support the relevance of the proposed two classes of DSB as a basis for the understanding of the cell response to ion irradiation. Importantly the density of DSB within DNA giant loops of around 2 Mbp size, i.e., on a micrometer scale, is identified as a key parameter for the description of radiation effectiveness. Further experimental and modeling work will be dedicated to test the general validity of this working hypothesis.

REFERENCES

1. Olive PL, Banath JP, Sinnott LT. phosphorylated histone H2AX in spheroids, tumors, and tissues of mice exposed to etoposide and 3-amino-1,2,4-benzotriazine-1,3-dioxide. Cancer Res 2004; 64:5363–9.

2. Banath JP, Macphail SH, Olive PL. Radiation sensitivity, H2AX phosphorylation, and kinetics of repair of DNA strand breaks in irradiated cervical cancer cell lines. Cancer Res 2004; 64:7144–9.

3. Macphail SH, Banath JP, Yu TY, Chu EH, Lambur H, Olive PL. Expression of phosphorylated histone H2AX in cultured cell lines following exposure to x-rays. Int J Radiat Biol 2003; 79:351–8.

4. Wada S, Van KT, Kobayashi Y, Funayama T, Ogihara K, Ueno S et al. Prediction of cellular radiosensitivity from DNA damage induced by gamma-rays and carbon ion irradiation in canine tumor cells. J Vet Med Sci 2005; 67:1089–95.

5. Mirzayans R, Severin D, Murray D. Relationship between DNA double-strand break rejoining and cell survival after exposure to ionizing radiation in human fibroblast strains with differing ATM/P53 status: Implications for evaluation of clinical radiosensitivity. Int J Radiat Oncol Biol Phys 2006; 66:1498–505.

6. Taucher-Scholz G, Heilmann J, Kraft G. Induction and rejoining of DNA double-strand breaks in CHO cells after heavy ion irradiation. Adv Space Res 1996; 18:83–92.

7. Asaithamby A, Uematsu N, Chatterjee A, Story MD, Burma S, Chen DJ. Repair of HZE-particle-induced DNA double-strand breaks in normal human fibroblasts. Radiat Res 2008; 169:437–46.

8. Fowler JF. Is repair of DNA strand break damage from ionizing radiation second-order rather than first-order? A simpler explanation of apparently multiexponential repair. Radiat Res 1999; 152:124–36.

9. Lobrich M, Cooper PK, Rydberg B. Non-random distribution of DNA double-strand breaks induced by particle irradiation. Int J Radiat Biol 1996; 70:493–503.

10. Carabe-Fernandez A, Dale RG, Paganetti H. Repair kinetic considerations in particle beam radiotherapy. Br J Radiol 2011; 84:546–55.

11. Shibata A, Conrad S, Birraux J, Geuting V, Barton O, Ismail A et al. Factors determining DNA double-strand break repair pathway choice in G2 phase. EMBO J 2011; 30:1079–92.

12. Belli M, Cherubini R, Finotto S, Moschini G, Sapora O, Simone G et al. RBE-LET relationship for the survival of V79 cells irradiated with low energy protons. Int J Radiat Biol 1989; 55:93–104.

13. Goodhead DT, Belli M, Mill AJ, Bance DA, Allen LA, Hall SC et al. Direct comparison between protons and alpha-particles of the same LET: I. Irradiation methods and inactivation of asynchronous V79, HeLa and C3H 10T1/2 cells. Int J Radiat Biol 1992; 61:611–24.

14. Friedrich T, Durante M, Scholz M. Particle species dependence of cell survival RBE: evident and not negligible. Acta Oncol 2013; 52:589–603.

15. Kramer M, Kraft G. Calculations of heavy-ion track structure. Radiat Environ Biophys 1994; 33:91–109.

16. Scholz M, Kraft G. Track structure and the calculation of biological effects of heavy charged particles. Adv Space Res 1996; 18:5–14.

17. Nikjoo H, Uehara S, Wilson WE, Hoshi M, Goodhead DT. Track structure in radiation biology: theory and applications. Int J Radiat Biol 1998; 73:355–64.

18. Heilmann J, Taucher-Scholz G, Haberer T, Scholz M, Kraft G. Measurement of intracellular DNA double-strand break induction and rejoining along the track of carbon and neon particle beams in water. Int J Radiat Oncol Biol Phys 1996; 34:599–608.

19. Kramer M, Kraft-Weyrather W, Scholz M. The increased biological effectiveness of heavy charged particles: from radiobiology to treatment planning. Tech Cancer Res Treat 2003; 2:427–36.

20. Hada M, Georgakilas AG. Formation of clustered DNA damage after high-LET irradiation: A review. J Radiat Res 2008; 49:203–10.

21. Okayasu R. Repair of DNA damage induced by accelerated heavy ions—A mini review. Int J Cancer 2012; 130:991–1000.

22. Scholz M, Kellerer AM, Kraft-Weyrather W, Kraft G. Computation of cell survival in heavy ion beams for therapy. The model and its approximation. Radiat Environ Biophys 1997; 36:59–66.

23. Elsasser T, Scholz M. Cluster effects within the local effect model. Radiat Res 2007; 167:319–29.

24. Elsasser T, Kramer M, Scholz M. Accuracy of the local effect model for the prediction of biologic effects of carbon ion beams in vitro and in vivo. Int J Radiat Oncol Biol Phys 2008; 71:866–72.

25. Elsasser T, Weyrather WK, Friedrich T, Durante M, Iancu G, Kramer M et al. Quantification of the relative biological effectiveness for ion beam radiotherapy: direct experimental comparison of proton and carbon ion beams and a novel approach for treatment planning. Int J Radiat Oncol Biol Phys 2010; 78:1177–83.

26. Yokota H, Van Den Engh G, Hearst JE, Sachs RK, Trask BJ. Evidence for the organization of chromatin in megabase pair-sized loops arranged along a random walk path in the human G0/G1 interphase nucleus. J Cell Biol 1995; 130:1239–49.

27. Solovjeva L, Svetlova M, Stein G, Chagin V, Rozanov Y, Zannis-Hadjopoulos M et al. Conformation of replicated segments of chromosome fibres in human S-phase nucleus. Chromosome Res 1998; 6:595–602.

28. Rogakou EP, Pilch DR, Orr AH, Ivanova VS, Bonner WM. DNA double-stranded breaks induce histone H2AX phosphorylation on serine 139. J Biol Chem 1998; 273:5858–68.

29. Friedrich T, Scholz U, Elsasser T, Durante M, Scholz M. Calculation of the biological effects of ion beams based on the microscopic spatial damage distribution pattern. Int J Radiat Biol 2012; 88:103–7.

30. Friedrich T, Durante M, Scholz M. Modeling cell survival after photon irradiation based on double-strand break clustering in megabase pair chromatin loops. Radiat Res 2012; 178:385–94.

31. Neumaier T, Swenson J, Pham C, Polyzos A, Lo AT, Yang P et al. Evidence for formation of DNA repair centers and dose-response nonlinearity in human cells. Proc Natl Acad Sci U S A 2012; 109:443–8.

32. Blocher D. DNA double strand breaks in ehrlich ascites tumour cells at low doses of x-rays. I. Determination of induced breaks by centrifugation at reduced speed. Int J Radiat Biol Relat Stud Phys Chem Med 1982; 42:317–28.

33. Prise KM, Pinto M, Newman HC, Michael BD. A review of studies of ionizing radiation-induced double-strand break clustering. Radiat Res 2001; 156:572–6.

34. Stenerlöw B, Karlsson KH, Cooper B, Rydberg B. Measurement of prompt DNA double-strand breaks in mammalian cells without including heat-labile sites: results for cells deficient in nonhomologous end joining. Radiat Res 2003; 159:502–10.

35. Taucher-Scholz G, Heilmann J, Schneider M, Kraft G. Detection of heavy-ion-induced DNA double-strand breaks using static-field gel electrophoresis. Radiat Environ Biophys 1995; 34:101–6.

36. Belli M, Cherubini R, Dalla VM, Dini V, Moschini G, Signoretti C et al. DNA DSB induction and rejoining in v79 cells irradiated with light ions: a constant field gel electrophoresis study. Int J Radiat Biol 2000; 76:1095–104.

37. Stenerlöw B, Hoglund E, Carlsson J, Blomquist E. Rejoining of DNA fragments produced by radiations of different linear energy transfer. Int J Radiat Biol 2000; 76:549–57.

38. Schneider M, Taucher-Scholz G, Heilmann J, Kraft G. Combination of static-field gel electrophoresis and densitometric scanning for the determination of radiation-induced DNA double-strand breaks in CHO cells. Radiat Environ Biophys 1994; 33:111–24.

39. Rydberg B. radiation-induced heat-labile sites that convert into DNA double-strand breaks. Radiat Res 2000; 153:805–12.

40. Sachs RK, Van Den Engh G, Trask B, Yokota H, Hearst JE. A random-walk/giant-loop model for interphase chromosomes. Proc Natl Acad Sci U S A 1995; 92:2710–4.

41. Johnston PJ, Olive PL, Bryant PE. Higher-order chromatin structure-dependent repair of DNA double-strand breaks: modeling the elution of DNA from nucleoids. Radiat Res 1997; 148:561–7.

42. Ostashevsky J. A Polymer model for the structural organization of chromatin loops and minibands in interphase chromosomes. Mol Biol Cell 1998; 9:3031–40.

43. Mateos-Langerak J, Bohn M, De LW, Giromus O, Manders EM, Verschure PJ et al. Spatially Confined folding of chromatin in the interphase nucleus. Proc Natl Acad Sci U S A 2009; 106:3812–7.

44. Hoglund H, Stenerlöw B. Induction And rejoining of DNA double-strand breaks in normal human skin fibroblasts after exposure to radiation of different linear energy transfer: possible roles of track structure and chromatin organization. Radiat Res 2001; 155:818–25.

45. Alloni D, Campa A, Belli M, Esposito G, Mariotti L, Liotta M et al. Monte Carlo evaluation Of DNA fragmentation spectra induced by different radiation qualities. Radiat Protect Dosim 2011; 143:226–31.

46. Singh SK, Bencsik-Theilen A, Mladenov E, Jakob B, Taucher-Scholz G, Iliakis G. Reduced Contribution of thermally labile sugar lesions to DNA double strand break formation after exposure to heavy ions. Radiat Oncol 2013; 8:77.

47. Ratnayake RK, Semenenko VA, Stewart RD. Retrospective analysis of double-strand break rejoining data collected using warm-lysis PFGE protocols. Int J Radiat Biol 2005; 81:421–8.

48. Belli M, Cera F, Cherubini R, Haque AM, Ianzini F, Moschini G et al. Inactivation and mutation induction in v79 cells by low energy protons: Re-evaluation of the results at the LNL facility. Int J Radiat Biol 1993; 63:331–7.

49. Sutherland BM, Bennett PV, Sidorkina O, Laval J. Clustered DNA damages induced in isolated DNA and in human cells by low doses of ionizing radiation. Proc Natl Acad Sci U S A 2000; 97:103–8.

50. Nikjoo H, O'Neill P, Wilson WE, Goodhead DT. Computational approach for determining the spectrum of DNA damage induced by ionizing radiation. Radiat Res 2001; 156:577–83.

51. Ottolenghi A, Merzagora M, Tallone L, Durante M, Paretzke HG, Wilson WE. The quality of DNA double-strand breaks: a Monte Carlo simulation of the end-structure of strand breaks produced by protons and alpha particles. Radiat Environ Biophys 1995; 34:239–44.

52. Ward JF. The Complexity Of DNA Damage: Relevance To Biological Consequences. Int J Radiat Biol 1994; 66:427–32.

53. Asaithamby A, Hu B, Chen DJ. Unrepaired clustered DNA lesions induce chromosome breakage in human cells. Proc Natl Acad Sci U S A 2011; 108:8293–8.

54. Gauter B, Zlobinskaya O, Weber KJ. Rejoining of radiation-induced DNA double-strand breaks: pulsed-field electrophoresis analysis of fragment size distributions after incubation for repair. Radiat Res 2002; 157:721–33.

55. Radulescu I, Elmroth K, Stenerlöw B. Chromatin organization contributes to non-randomly distributed double-strand breaks after exposure to high-LET radiation. Radiat Res 2004; 161:1–8.

56. Johnston PJ, Macphail SH, Banath JP, Olive PL. Higher-order chromatin structure-dependent repair of DNA double-strand breaks: factors affecting elution of DNA from nucleoids. Radiat Res 1998; 149:533–42.

57. Johnston PJ, Macphail SH, Stamato TD, Kirchgessner CU, Olive PL. Higher-order chromatin structure-dependent repair of DNA double-strand breaks: involvement of the v(d)j recombination double-strand break repair pathway. Radiat Res 1998; 149:455–62.

58. Friedland W, Jacob P, Paretzke HG, Ottolenghi A, Ballarini F, Liotta M. Simulation of light ion induced DNA damage patterns. Radiat Prot Dosimetry 2006; 122:116–20.

59. Goodarzi AA, Jeggo P, Lobrich M. The influence of heterochromatin on DNA double strand break repair: getting the strong, silent type to relax. DNA Repair (Amst) 2010; 9:1273–82.

60. Kinner A, Wu W, Staudt C, Iliakis G. Gamma-H2AX In recognition and signaling of DNA double-strand breaks in the context of chromatin. Nucleic Acids Res 2008; 36:5678–94.

61. Li Y, Qian H, Wang Y, Cucinotta FA. A stochastic model of DNA fragments rejoining. Plos One 2012; 7:E44293.

62. Pinto M, Prise KM, Michael BD. A Monte Carlo model of DNA double-strand break clustering and rejoining kinetics for the analysis of pulsed-field gel electrophoresis data. Radiat Res 2004; 162:453–63.

63. Pinto M, Prise KM, Michael BD. Evidence for complexity at the nanometer scale of radiation-induced DNA dsbs as a determinant of rejoining kinetics. Radiat Res 2005; 164:73–85.

64. Friedland W, Dingfelder M, Kundrat P, Jacob P. Track structures, DNA targets and radiation effects in the biophysical Monte Carlo simulation code PARTRAC. Mutat Res 2011; 711:28–40.

65. Friedland W, Jacob P, Kundrat P. Stochastic simulation of DNA double-strand break repair by non-homologous end joining based on track structure calculations. Radiat Res 2010; 173:677–88.

66. Friedland W, Kundrat P, Jacob P. Stochastic modelling of DSB repair after photon and ion irradiation. Int J Radiat Biol 2012; 88:129–36.